JOURNAL OF MATERIALS SCIENCE **36** (2001) 219–224

Optical second harmonic generation in $CsLiB_6O_{10}$ nanocrystallites incorporated to the olygoether photopolymer matrices induced by acoustical field

A. MEFLEH, S. BENET
LP2A, Université de Perpignan, 52, Avenue de Villeneuve, 66860 Perpignan, France

A. MAJCHROWSKI
Solid State Department Czestochowa, PL-42217, ul. Gombrowicza 1/144, Czestochowa, Poland

I. V. KITYK
Institute of Applied Physics WAT, 2 Kaliskiego Str., 00-908, Warsaw, Poland
E-mail: i.kityk@wsp.czest.pl

Optical second harmonic generation in $CsLiB_6O_{10}$ (CLBO) large-sized nanocrystallites (15–40 nm) incorporated into the olygoether photopolymer matrices has been found at liquid helium temperature (LHeT). The second harmonic generation (SHG) has been measured for the source wavelength of the YAG : Nd laser ($\lambda = 1.06$ μm). Increasing acoustical power (up to 18.1 W/cm^2) and acoustical frequencies at 14 kHz give maximal values of the output SHG. The measured SHG χ_{222} tensor component was comparable with the one for the traditional nonlinear optical crystals such as KH_2PO_4, $KTiOPO_4$, $LiNbO_3$. With decreasing temperature below 28 K the acoustically induced SHG signal strongly increases. A correlation between the acoustically induced SHG and low-frequency Raman modes has been found. The maximal acoustically induced SHG has been observed for the nanocrystallite concentration about 3.1% (in weighting units) and the crystallite sizes lying within the 35–40 nm. The SHG tensor coefficients were higher than for the proper CLBO crystals at least on the 13%. Advantageous and drawbacks of the presented model are discussed. The theory of the observed phenomena is explained on the ground of *ab initio* band energy calculations with taking into account of anharmonic electron-phonon interactions. © *2001 Kluwer Academic Publishers*

1. Introduction

Recently one can see increasing interest to nanocrystals due to a possibility of enhancement of the nonlinear optical coefficients by varying their sizes [1–5]. Wide-energy gap nanocrystals are of especial interest because theoretical calculations [6, 7] predict possibility of essential enhancement the nonlinear optical susceptibilities. Among the new synthesized borate crystals it is necessary to name the following: BBO, YCOB, KAB, BIBO and LBO [8, 9]. However there remains a problem with their fabrication. In the references [8–10] linear- and nonlinear-optical properties of the new synthesized CLBO single crystals were discovered. These single crystals are absolutely insensitive to moisture and are very convenient for achievement of large-size (15–40 nm) nanocrystals. The specimens are transparent in visible and in the near IR spectral range (from 0.32 to 3.1 μm). Value of damage threshold is of about 2.9 GW/cm^2 for the nanosecond laser pulses and efficiency of the optical second harmonic generation (SHG) is higher than 50% for the YAG : Nd laser wavelength. Coming out from a similarity of the mentioned crystals to other borate crystals, for example to $Li_2B_4O_7$ single crystals [11], one can expect that the mentioned crystals should posses also good acoustical properties. Moreover simultaneous presence of the Li and Cs ions could stimulate different kinds of the acoustically-induced phenomena. At the same time the photopolymer oligoetheracrylate matrices possess also the good acoustooptical parameters [12] that could ensure a good transfer between the external acoustically induced properties.

At the same time the CLBO nanocrystals may be a good NLO chromophores for a possibility to be incorporated in different polymer matrices.

A wide application of the nanocrystallites is essentially restrained by the technological complications connected with a necessity of preparation the appropriate composites. Usually such composites are prepared like a film deposited on the dielectric subtract [13]. In

this case a main problem consists in a high light scattering background. To overgo this the guest-host polymer technique [14–16] may be applied. Such technique has been used in the Ref. 17 for fabrication of $Sn_2P_2S_6$ semiconductor nanocrystallites embedded in the oligoetheracrylate photopolymer matrices. It was shown that better technological parameters (lower light scattering losses, optical homogeneity, higher transparency etc) are achieved when the external electric field is applied [18].

The CLBO nanocrystals have essential advantageous comparing with other borates because for these materials technology of preparation the specimens with desired sizes has been good developed [19]. At the same time theoretical simulations predict [20] a possibility of appearance the large second-order nonlinear optical effects. Calculated electron charge density distribution in the oligoetheracrylate photopolymers [21–23] indicates on a good complementation of these polymers to the binary semiconductors because the appropriate (both electronic as well vibrations) matrix dipole moments are collinear.

The main reason of the present work consists in searching of ways for optimisation of the second-order nonlinear optical susceptibilites:

- nano-crystalline near-the-surface confinement;
- superposition of the particular nonlinear optical susceptibilities originating from the nanocrystallites and surrounding photopolymers;
- using of external acoustical treatment for enhancement of the nonlinear optical susceptibilities.

We will present experimental results for the acoustically SHG in the CLBO composites. In the Section 2 technology of specimen preparation and measurement setup is presented. Sec. 3 describes study of the acoustically-induced SHG. Theoretical simulations on a ground of *ab initio* pseudopotential calculations and the appropriate discussion are presented in the Sec. 4.

2. Experimental details

2.1. Sample preparation

The CLBO crystals were synthesized by the top-seeded solution growth method using self-flux. The raw materials were Cs_2CO_3 and Li_2CO_3. Stoichiometric ratio $Cs_2O : Li_2O : B_2O_3$ has been reduced to 1 : 1 : 5.6 in order to restrict viscosity of solution. The mixture was calcined and charged in a platinum crucible which was kept in the uniform hot zone of the furnace heated up to 900°C and then cooled down to the saturation temperature of 825°C. After holding at this temperature for 24 h they were slowly cooled down to 823°C at a rate of 0.1 K/h. The seed specimen was rotated at a speed of 10–20 rpm for both cases. The grown crystals were pulled out from the solution and then cooled down to the room temperature at a rate of 0.1 K/h. X-ray powder diffractometer control has shown that the space group of the CLBO crystals was I2d with lattice parameter $a = 10.495$ A, $c = 8.939$ A, $Z = 4$.

Control of the phase single crystalline homogeneity was carried out using DRON 5.0 X-ray diffractometer. After the single crystals have been crushed and melt both mechanically as well by ultrasound waves in order to obtain the nano-powder nanocrystallites.

The synthesized nanocrystalline samples had powder-like form with diameter sizes lying within the size ranges of 15–70 nm. The powder-like specimens were dissolved in the liquid oligoetheracrylate photopolymer matrices (more details see in the Ref. 17). The solidification process and electropoling homogenization have been carried out using a method described in the Ref. [17]. Nitrogen laser ($\lambda = 337$ nm) with the photon energy power about 35 W/cm^2 was used for the solidification.

Afterwards the LNB piezoelectric acoustical transducers have been attached to the investigated composition by a CYATYM glue. The equipment allows us continuously to vary specimen thickness within the 0.2–1.3 cm with the increment of the 0.1 mm. Homogenization of the mixture has been conducted using ultrasound mixing and crushing. Control of the specimen homogeneity was performed by an optical polarized method. We have revealed that deviation from the homogeneity was less than 3.6% through the specimen surface.

2.2. Measurement setup

The pumping was provided by picosecond pulses of $\lambda = 1.06$ μm of YAG : Nd laser ($\lambda = 1.06$ mm; $W =$ 30 MW; $\tau = 30$ ps). The acoustical signal power has been applied to the specimens by LNB piezoelectric transducers in the c_{66} prolonged tensor geometry with the varied acoustical frequencies (80 Hz–1.2 MHz). The photoinducing nitrogen and probing (YAG-Nd) laser light was polarized using rotating Fresnel polarizers and the output light intensities were detected using photomultipliers. The measurements were done in the single-pulse regime, with a pulse frequency repetition of 12 Hz and the tunable pulse duration within the 26–50 ps. Such short-time kinetics allows us to eliminate the specimen heating. The pumping laser beams have been scanned over the specimen surface in order to eliminate the specimen non-homogeneity contributions. The measurements have been done both for the transmitted as well for the reflected light beam regime. For every thickness we have obtained more than 120 measured points for the transmitted T, reflected R and scattered R_s light intensitites. Precision of the T and R evaluations was better than 5%.

Laser power beams have been diafragmed to obtain the light profile inhomogeneity (usually of the gaussian-like form) about 92% relatively to the maximum light intensity for the energy powers lying within the 0.75–2.75 GW/cm^2. Measurements devices both for the transparent and reflected channel have been synchronized. Statistical treatment using the χ^2 Student approach gives a reliability of the obtained data better than 0.03. Independent measurements of the SHG for the proper oligoether matrices have been done. The latter one was necessary to eliminate an influence of photopolymer matrix background, influence of linear absorption (245 cm^{-1}, $\lambda = 530$ nm) and of Fresnel reflection and have been taken into account during the evaluations of the PISHG. The choice of the oligoetheracrylate matrices is caused by relatively low value of

their proper SHG coefficient (below 0.002 pm/V) and close values of the corresponding refractive indices for the CLBO and the oligoetheracrylates (see for example ref. 24).

To exclude an influence of the hyper-Raman scattering superposing on the output SHG, we have carried out additional investigations of the scattered light up to 2600 cm^{-1}, starting from the wavelength $\lambda = 441$ nm. Hyper-Raman maximums within the 1200 cm^{-1}–1800 cm^{-1} spectral range possess intensities at least 9 times weaker than the transmitted light intensity. In the case of the Raman and hyper-Raman measurements we have used argon laser at 441 nm Ar^+ laser line and SPM-3 spectrometer. A position-sensitive photomultiplier was used to detect the integrated light scattering background.

The temperature has been varied within the 4.2–300 K range. Precision of the temperature stabilization was equal about ± 0.12 K. All the measured optical parameters were averaged over a great number of pulses (about 160–180) for every T point. The intensity of the laser beams was varied using neutral density filters. A delaying time between the pump and probe pulses was created using the $Li_2B_4O_7$ single crystalline plate.

3. Theoretical simulations of the acoustically induced effects

Calculations of the band electronic structure with taking into account of electron-phonon interactions have been performed in order to clarify the nature of acoustically-induced SHG. The evaluations have been used *ab initio* norm-conserving pseudopotential method [24] within the local density approximation (LDA).

The surrounding electropoled photopolymer environment has been taken into account using the extended quasi-Brillouine zone. At the beginning we separate contribution of the electron and vibration subsystems effectively contributing to the appropriate nonlinear optical susceptibilities. Phonon modes within the GdCOB chromophores have been calculated in a harmonic approximation:

$$d^2\Psi_k/dQ_k^2 + \left[4\pi^2\mu_k h^{-2}\Omega_k^2\right]\Psi_k = 0 \qquad (1)$$

where Ψ_k is a vibration-like wave function corresponding to k-th normal coordinate Q_k within the GdCOB nanocrystallites renormalized by the surrounding long-range amorphous-like background; μ_k denotes a reduced mass of the ions in the k-th phonon mode. Acoustical modes are especially interesting for this case, because they possess information concerning the particular crystallites as well surrounding photopolymer matrix. In this case second derivatives of the effective nanocrystalline potential renormalised by surrounding amorphouslike background play a dominant role in the observed phonon modes.

An eigen-energy of the k-th phonon mode was written in a form:

$$\Omega_k(\nu_k) = 2\Omega_{k0}(\nu_k + 1/2), \qquad (3)$$

where $\Omega_{k0} = (h/2\pi)(f_k/\mu_k)^{1/2}/2$ is an eigen-energy for the zero-point quasi-phonons and $\nu_k = 0, 1, 2, \ldots$ are phonon quantum numbers described by the following expressions:

$$\Psi_k(Q_k) = (2\Omega_{k0}/\pi)^{1/4}(2^{\nu_k}/\nu_k!)^{-1/2} \times \exp(-\Omega_{k0}Q_k 2)H_\nu((2\Omega_{k0})^{1/2}Q_k) \quad (4)$$

where $H_\nu(x)$ is a Hermite polynomial.

In order to perform a modeling of the acoustically-induced changes it is obviously that electron-phonon interactions should be considered, particularly for the low-frequency phonon modes that could be in frequency resonance with external acoustical waves. Calculations of electron-phonon anharmonic potential was carried out (this can be seen in the absorption spectra) in a nonlinear approximation similar as in the Ref. 17:

$$V_{e\text{-ph}}(r_i) = e^2 \sum_{\mathrm{ms}} M_{\mathrm{ms}}^{-1/2}\Big[Z_{\mathrm{ms}}(r_{\mathrm{s}} - u_{\mathrm{ms}})|r_{\mathrm{s}} - u_{\mathrm{ms}}|^{-3} - \sum_{\mathrm{m's'}} Z_{\mathrm{m's'}}(r_{\mathrm{s'}} - u_{\mathrm{m's'}})|r_{\mathrm{s'}} - u_{\mathrm{m's'}}|^{-3}\Big] \quad (5)$$

where M_{ms} and eZ_{ms} are effective ionic mass and charge for corresponding ions numbered by m and s, respectively. Both intra- as well internanocrystalline interactions are taken into account. Moreover two effective wavevectors have been introduced. The first one, traditional corresponds to the nanocrystallite units and the second represents molecular sphere originating from photopolymer background. Influence of the interface region (between the nanocrystallites and photopolymer backgrounds) has been extracted by performing a derivative procedure that eliminates possible potential jumps on the interface boarders. The $\mathbf{u}_{\mathrm{ms,m's'}}$ vector is a relative displacement of two ions from their equilibrium positions $\mathbf{r}_{\mathrm{s}}$ and $\mathbf{r}_{\mathrm{s'}}$. A probability of a one-phonon transition induced by the phonon of a frequency Ω_k is equal to:

$$\Xi(\Omega_k) = 4(h/2\pi)^{-2}c^{-3}H^{-1}g^{-1}(r_i)(E_{\mathrm{el}} - \Omega_k)^2\Theta(\Omega_k) \qquad (6)$$

where H is a sum of the η and ξ level widths, E_{el} is an electron transition energy, Ω_k denotes a phonon energy and $g(r_i)$ is a degeneration degree of the corresponding electron energy levels. The parameter $\Theta(\Omega_k)$ is equal to:

$$\Theta(\Omega_k) = \sum_\eta g(\eta)\sum_\xi g(\xi)\Bigg|\Bigg\{\sum_\varphi \langle\eta, \eta_\Omega|V_{e\text{-ph}}(\boldsymbol{r}_i)|\varphi, \eta_{\Omega+1}\rangle\langle\varphi|\boldsymbol{d}|\xi\rangle(E_\xi - E_\eta + \Omega_k)^{-1} + \sum_\varphi \langle\eta|\boldsymbol{d}|\varphi\rangle\langle\varphi, \eta_\Omega|V_{e\text{-ph}}(\boldsymbol{r}_i)|\xi, \eta_{\Omega-1}\rangle \times (E_\xi - E_\eta - \Omega_k)^{-1}\Bigg\}\Bigg|^2\theta, \qquad (7)$$

here η and the ξ are lower and upper electron energy levels, respectively; φ denotes a virtual electron state, **d** is an electric dipole moment for a given spectral transition. The summation is performed over all degenerated

initial and final states. Orthogonalization to the highly delocalized states has been carried out by the method described in the Ref. 17. The symbol θ denotes an averaging over the all occupied phonon states for phonons with frequency Ω_k. The symmetric phonon vibrations included in the electron-phonon interaction (see Equation 5) are renormalized by the normal coordinates to a form:

$$\Theta(\Omega_k) = C^{\gamma}_{\eta\xi}\left(r^{\Delta}_{\lambda}\right) C^{\gamma'}_{\eta\xi}\left(r^{\Delta'}_{\lambda'}\right) \operatorname{Im} G^{\gamma\gamma'}_{\Delta\Delta'}\left(r^{\Delta}_{\lambda}, \Omega^2_k\right) \quad (8)$$

where $G^{\gamma\gamma'}_{\Delta\Delta'}(r^{\Delta}_{\lambda})$ is a Green function (γ and γ' are numbers of interacting coordination sphere) defined as:

$$G^{\gamma\gamma'}_{\Delta\Delta'}\left(r^{\Delta}_{\lambda}\right) = \sum_{\varphi} \{\langle\eta|V_{\text{e-ph}}(\boldsymbol{r}_i)|\varphi\rangle\langle\varphi|\boldsymbol{d}|\xi\rangle + \langle\eta|\boldsymbol{d}|\varphi\rangle\langle\varphi|V_{e\text{-ph}}(\boldsymbol{r}_i)|\xi\rangle\}(E_{\xi} - E_{\eta})^{-1} \quad (9)$$

The Green function calculations are carried out for the perfect lattice renormalized by amorphous-like photopolymer environment with taking into account of the given nanocrystallite sizes by performing summation over 75 **k**-points in the irreducible part of the quasi-Brillouin zone. The resulting expression is given below:

$$G^{\gamma\gamma'}_{\Delta\Delta'}\left(r^{\Delta}_{\lambda}, \Omega^2_k\right) = \sum_{\Omega} K^{\gamma'}_{\Delta'}\left(r^{\Delta}_{\lambda}\right) K^{\gamma}_{\Delta}\left(r^{\Delta}_{\lambda}\right)\left(\Omega^2_k - \Omega^2 - i\delta\right)^{-1} \quad (10)$$

where the coordinates $K^{\gamma}_{\Delta}(r^{\Delta}_{\lambda})$ are obtained for a given quasi-phonon type from the electron states averaging. The acoustically-induced lattice perturbation into the Green functions has been done using a deformation localization that allows us to use the Dyson relations:

$$G^{\gamma\gamma'}_{\Delta\Delta'}(1) = G^{\gamma\gamma'}_{\Delta\Delta'}(0) + G^{\gamma\gamma'}_{\Delta\Delta'}(0) U G^{\gamma\gamma'}_{\Delta\Delta'}(1) \quad (11)$$

where $G^{\gamma\gamma'}_{\Delta\Delta'}(0)$ and $G^{\gamma\gamma'}_{\Delta\Delta'}(1)$ are the Green functions for ideal and acoustically perturbed systems, respectively. From the mentioned equation we have obtained the modified electron-phonon wavefunctions for calculation of the intra-the-cluster electrostatic potential and corresponding phonon modes before and after applying the acoustical waves.

Afterwards interaction of the acoustical modes with the appropriate phonon modes has been taken into account. In the Fig. 1 are presented changes of effective electrostatic potential contours and of the effective low-frequency acoustical modes under influence of external acoustical field. One can clearly see that the applied acoustical field essentially changes electrostatic potential distribution. The typical quasi-phonon modes assisting in the appearance of the non-centrosymmetry are presented. It is necessary to point out that the more essential changes were expected for the temperature about the 4.2 K. Appearance of additional non-centrosymmetry in the electrostatic potential distribution is a main requirement for enhancement of the nonlinear optical properties. From the Fig. 1 such acoustically-induced non-centrosymmetry is shown unambiguously.

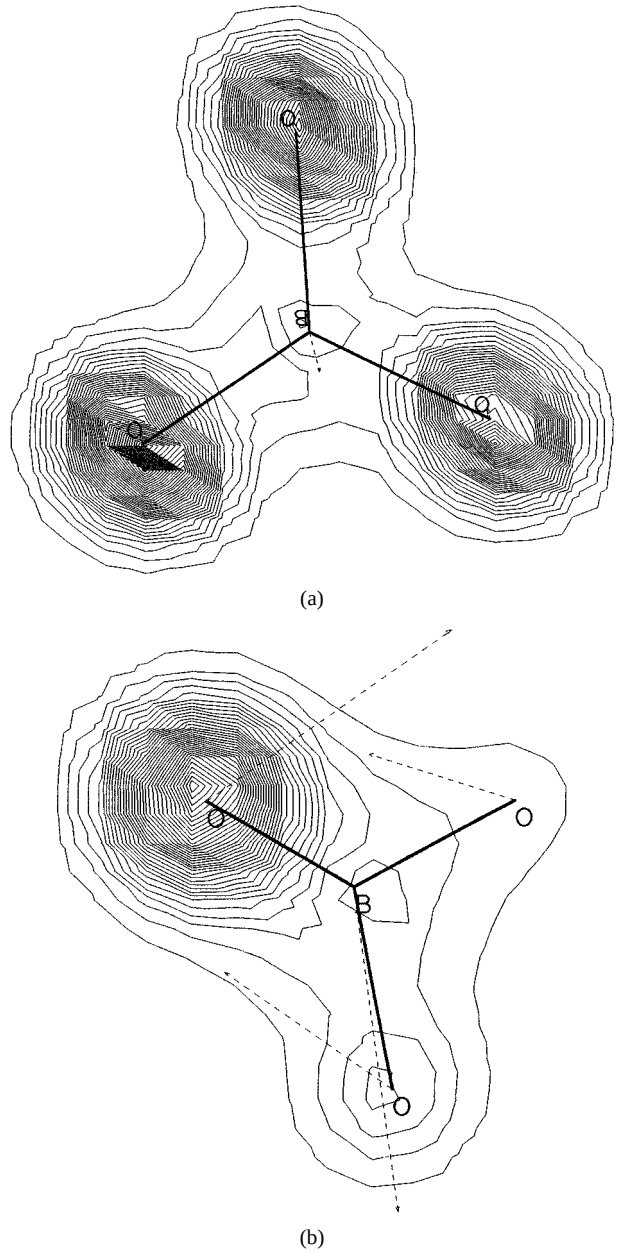

Figure 1 Fragment of the [BO_3] cluster of the CLBO nanocrystallites electrostatic potential distribution together with active phonon modes. The later are indicated by the arrows. (a) Before applying of the acoustical field; b) after the applying field. The simulations are presented for the LHeT.

4. Experimental results and discussion

From the performed mathematical simulations one can see that acoustical field stimulates non-centrosymmetry in electrostatic potential distribution determining the polar third rank tensors. Lets consider experimental dependence of the SHG versus nanocrystallite sizes and acoustical power (see Fig. 2). Essential SHG signal has been observed only below 28 K. Thus we present only the data at LHeT when the output SHG signal is maximal.

One can see essentially nonlinear dependence of the SHG versus nanocrystallite concentration and

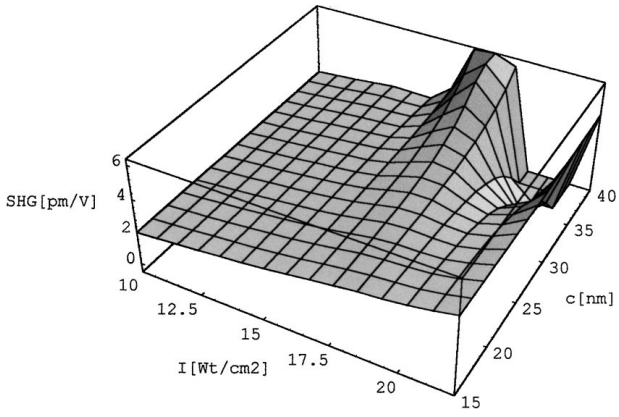

Figure 2 Dependence of the acoustically-induced SHG versus nanocrystallite sizes c and acoustical power W at LHeT.

acoustical power. For low acoustical powers (below 6 W/cm^2) and for nanocrystallite sizes within the 25–40 nm quasi-linear increase of the output SHG (for the χ_{222} tensor geometry) with increasing acoustical power and nanocrystallite sizes is observed. For the sizes higher than 38 nm a saturation of the SHG is observed. Moreover for acoustical power higher than 19 W/cm^2 drastic abrupt of the SHG maximum appears. The maximum value of the χ_{222} tensor component is at least 13% higher than the maximal SHG tensor value for the proper CLBO single crystals.

The observed dependencies of the acoustically induced SHG as well appropriate *ab initio* cluster geometry optimisation unambiguously indicate on a fundamental role played by acoustical waves in increasing electron-phonon interactions and appearance of the corresponding electrostatic potential non-centrosymmetry. In order to confirm this prediction, particularly about the central role of the phonon modes) independent measurements of the Raman spectra (see Fig. 3) have been carried out. The main goal was to evaluate changes of the low-frequency phonons under influence of external acoustical field. One can clearly see an essential

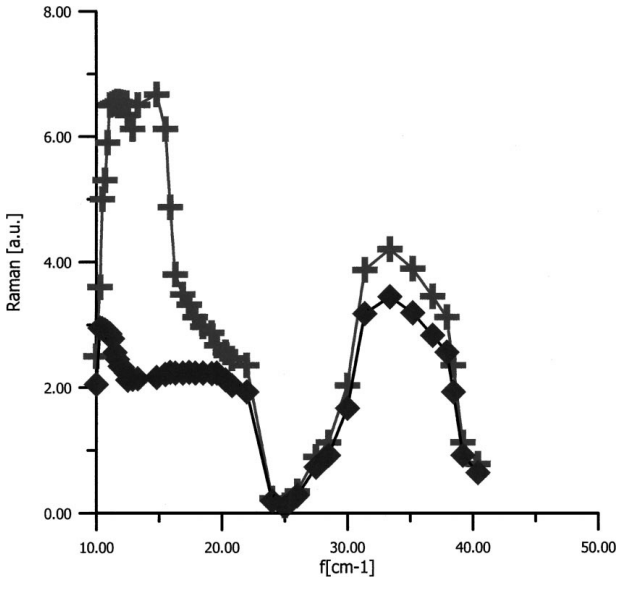

Figure 3 Photoinduced Raman spectral changes at different level of the external acoustical fields: ✦ - 6; ♦ - 20 Wt/cm^2 at LHeT.

rearrangement of the Raman mode at 14.1–15.3 cm^{-1} with increasing acoustical power. This ones can serve as a main prove that the low-frequency phonons stimulated by external fields play key role in the observed phenomena.

The observed behavior is caused by anharmonic electron-quasi-phonon interactions within and outside the particular nanocrystallites. The more typical vibrations contributing to the output susceptibilities are presented in the Fig. 3 by arrows. It is necessary to add that the observed acoustically induced SHG coefficients were at least 7% higher than for the photoinduced effects without the acoustical field [19, 20]. Therefore one can say about essentially new way for enhancement of the nonlinear optical coefficients in such kinds of composites.

5. Conclusions

Acoustically induced optical SHG in the large-sized CLBO nanocrystallites incorporated into the olygoetheracrylate photopolymer matrices has been revealed at LHeT. *Ab initio* band energy structure calculation shows that origin of the observed phenomena consists in appearance of a non-centrosymmetry in electrostatic potential distribution due to interaction with externally stimulated acoustical phonons of the CLBO nanocrystallite interfaces and surrounding photopolymer matrices. Essential influence of acoustically induced electron-phonon interactions is confirmed by measurement of acoustically induced Raman spectra. Nonlinear dependence of the acoustically-induced SHG versus nanocrystallite concentration and acoustical power is observed. An increase of the output SHG (for the χ_{222} tensor geometry) has been observed for the low acoustical powers up to 18.1 W/cm^2 and nanocrystallite sizes about 38 nm. With the next increase of the acoustical power the SHG abruptly decreases.

The maximal value of the output SHG (about 4.1 pm/V) is comparable with the traditional nonlinear optical crystals such as KH_2PO_4, $KTiOPO_4$, $LiNbO_3$ [18].

References

1. C. R. KAGAN, C. B. MURRAY, M. NIRMAL and M. G. BAWENDI, *Phys. Rev. Lett.* **76** (1996) 1517.
2. A. MEWS, A. V. KADAVANICH, U. BANIN and A. P. ALIVISATOS, *Phys. Rev.* **B53** (1996) 13242.
3. D. J. NORRIS and M. G. BAVENDI, *J. Chem. Phys.* **103** (1995) 5260.
4. *Idem., Phys. Rev.* **B53** (1996) 16338.
5. N. A. HILL and K. B. WHALEY, *Phys. Rev. Lett.* **75** (1995) 1130.
6. R. W. SCHOENLEIN, D. M. MITTLEMAN, J. J. SHIANG, A. P. ALIVISATOS and C. V. SHANK, *ibid.* **70** (1993) 1014.
8. C. CHEN, B. WU, A. JIANG and G. YOU, *Sci. Sin.* **B28** (1985) 235; H. HELLWIG, J. LIEBERTZ and L. BOHATY, *Solid State Communic.* **109** (1999) 249.
9. C. CHEN, Y. WU, A. JIANG, B. WU, G. YOU, R. LI and S. LIN, *JOSA* **B6** (1989) 616; Z. G. HU, T. HIGASHIYAMA, M. YOSHIMURA, YK YAP, Y. MORI and T. SASAKI, *Jap. Journ. Appl. Physics* **37** (1998) L1093; T. SASAKI, Y. MORI, I. KURODA, S. NAKAJIMA, K. YAMAGUCHI

and S. WATANABE, *Acta Cryst.* **C51** (1995) 2222; Q. YE and B. H. T. CHAI, *Journ of Crystal Growth* **197** (1999) 228.
10. K. BAI and S. T. JUNG, *Journ. Crystal Growth* **186** (1998) 612.
11. YA. O. DOVGII, I. V. KITYK and YA. V. BURAK. *Phys. Stat. Sol.* **V.180B** (1993) P.K57-60.
12. R. I. MERWINSKII, I. V. KITYK, M. MAKOWSKA-JANUSIK, J. STRAUBE, M. MATUSIEWICZ and J. KASPERCZYK, *Optical Materials* **6** (1996) 239.
13. E. B. NOWIKOW, Problems of separation nanocrystallite by sizes. Preprint Inst. Nadtw.Materialow, AN USSR – 156, 1990, 65 p.
14. "Nonlinear Optical Effects in Organic Polymers," NATO ASI Series, Series E: Applied Sciences, Vol. 162, edited by J. Messier, F, Kajzar, P. Prasad and D. Ulrich (Kluwer Academic Publishers, Dordrecht, 1989).
15. "Materials for Nonlinear Optics," American Chemical Society, ACS Symposium Series, Vol. 455, edited by S. R. Marder, J. E. Sohn and G. D. Stucky (ACS, Washington, DC, 1991).
16. M. KUZYK and C. POGA, "Molecular Nonlinear Optics" (Academic Press, NY., 1994) ch. 7, p. 209.
17. I. V. KITYK, R. I. MERWINSKII, J. KASPERCZYK and S. JOSSI, *Materials Letters* **27** (1996) 233; B. SAHRAOUI, I. V. KITYK, X. N. PHU, A. GORGUES and P. HUDHOMME, *Phys. Rev.* **B59** (1999) 9229.
18. J. ZYSS and D. S. CHEMLA, "Quantum Electronics (Principles and Applications)," Vols. 1 and 2 (Academic Press, New York, 1987).
19. A. MEFLEH, S. BENET, B. SAHRAOUI, H. KADDOURI, M. MAKOWSKA-JANUSIK and I. V. KITYK, *Optical Materials*. **13** (1999) 339.
20. A. MEFLEH, S. BENET, B. SAHRAOUI, J. KASPERCZYK, J. BERDOWSKI, M. MAKOWSKA-JANUSIK and I. V. KITYK, *Proc. SPIE* **2021** (1999). 234.
21. M. CZERWINSKI, J. BIELIENINIK, J. NAPIERALSKI, I. V. KITYK, J. KASPERCZYK and R. I. MERWINSKII. *Europ. Polym. Journ.* **33** (1997) 1441.
22. B. SAHRAOUI, I. V. KITYK, M. CZERWINSKI and J. KASPERCZYK, *High Performance Polymers* **9** (1997) 51.
23. M. CZERWINSKI, R. I. MERWINSKII, M. KULESZA, I. V. KITYK and J. KASPERCZYK, *Mater. Chem. and Physics* **56** (1998) 713.
24. O. G. PETRENKO, R. I. MERVINSKII and I. V. KITYK, *J. Opt. Technol.* **62** (1995) 123.

Received 3 June 1999
and accepted 5 May 2000